AGU PUBLICATIONS

JGR

Journal of Geophysical Research: Planets

RESEARCH ARTICLE
10.1002/2015JE004860

Key Points:
- Referring to empirical densities is not safe to evaluate equilibrium states
- Onset diameter of equilibrium can be used to deduce relative surface ages
- Crater populations in equilibrium do not all follow uniform spatial distribution

Supporting Information:
- Text S1, Figures S1–S5, and Tables S1 and S2

Correspondence to:
Z. Xiao,
zyxiao@cug.edu.cn

Citation:
Xiao, Z., and S. C. Werner (2015), Size-frequency distribution of crater populations in equilibrium on the Moon, *J. Geophys. Res. Planets, 120*, 2277–2292, doi:10.1002/2015JE004860.

Received 26 MAY 2015
Accepted 10 NOV 2015
Accepted article online 13 NOV 2015
Published online 28 DEC 2015

Size-frequency distribution of crater populations in equilibrium on the Moon

Zhiyong Xiao[1,2] and Stephanie C. Werner[1,3]

[1]Centre for Earth Evolution and Dynamics, University of Oslo, Oslo, Norway, [2]Now at School of Earth Sciences, China University of Geosciences, Wuhan, China, [3]Department of Geosciences, University of Oslo, Oslo, Norway

Abstract Overprinting of craters by subsequent impacts and topographic degradation complicates crater statistics, especially for old surfaces and small-diameter crater populations. A crater population is regarded as in equilibrium at a particular crater size when smaller craters are being produced at the same rate at which they are being destroyed. Evaluating the equilibrium state of crater populations is challenging, and empirical equilibrium densities are frequently inferred. By performing careful crater counts and cross comparisons on several lunar surfaces, we study the size-frequency distributions (SFD) for the crater populations, which have portions in equilibrium. The results are one of the few observational constraints on the SFD of crater populations in equilibrium, showing that referring to empirical equilibrium densities is not safe for evaluating the equilibrium states of crater populations. Equilibrium densities are not positively correlated with the ages of crater populations, and some populations in equilibrium have crater densities less than those previously believed to represent equilibrium conditions. Besides the SFD of the production population, different crater removal rates at different diameters also affect the SFD of crater populations in equilibrium. The equilibrium onset diameter (D_{eq}) of a crater population can be translated to model ages because older populations have larger D_{eq}, and those for same-aged surfaces are comparable. We show that the crater populations studied here are in equilibrium at much smaller diameters than those predicted for same-aged surfaces by crater degradation models, thus indicating lower crater degradation rates on the Moon, and/or younger ages of the counting areas.

1. Introduction

Only limited samples returned by the Apollo and Luna missions and a few meteorites ejected from unknown places of the Moon have provided radiometric ages for the lunar surface. Impact crater statistics is the major tool used in dating lunar surfaces because crater density and size-frequency distribution (SFD) can be translated to relative and absolute model ages [*Neukum*, 1983]. The reliability of crater statistics is based on the premise that all the craters formed since the formation of the studied surface (i.e., production population) [*Neukum,* 1983] are included in the statistics.

For planetary surfaces where impact cratering is the dominate geological process, the crater density at any crater diameter will eventually reach an upper limit due to continuous bombardment, after which the whole cratering history is no longer preserved, particularly in the smaller diameter crater populations [cf. *Melosh*, 1989; *Richardson*, 2009]. Without surface erosion processes such as volcanism, tectonism, aeolian, fluvial, or glacial activity, continuous mass wasting (e.g., landslides and topography diffusion), impact cratering, and its associated effects (e.g., direct overlapping, ejecta burial, and seismic shaking) would obliterate a substantial number of previously formed craters, with smaller craters being more heavily affected than larger ones [cf. *Basaltic Volcanism Study Project*, 1981]. For craters less than a given size in a crater population, when the production rate is exactly balanced by the removal rate in a statistical sense, that portion of the crater population is regarded as in equilibrium [*Gault*, 1970]. After reaching equilibrium, the observable crater density at smaller diameters exhibits a lower density than the produced crater population. For a given crater population, the diameter of the largest crater at which the population is in equilibrium is called the equilibrium onset diameter (D_{eq}). Larger craters (i.e., $D > D_{eq}$) are not in equilibrium and represent the production crater population. Age determination using crater statistics should always be performed at diameter ranges larger than D_{eq}, otherwise, misleading ages would result [e.g., *Gault*, 1970].

Although the concept of crater equilibrium was established in the 1960s [*Shoemaker et al.,* 1969; *Gault*, 1970] and the SFD of crater populations in equilibrium were well modeled by considering different production

populations [e.g., *Richardson*, 2009], disputes about whether or not equilibrium actually occurred on the Moon or other solar system bodies have lasted for decades [e.g., *Gault*, 1970; *Woronow*, 1977; *Hartmann*, 1984; *Chapman and McKinnon*, 1986; *Hartmann and Gaskell*, 1997; *Richardson*, 2009]. From the various preservation states of impact craters on solar system bodies that are caused by continuous cratering and degradation, it seems probable that crater populations on many surfaces of planetary bodies do reach equilibrium to some diameter. Indeed, every surface on the Moon that is old enough (e.g., at least for surfaces that have comparable ages with Tycho; [*Shoemaker et al.,* 1969]) has reached equilibrium for craters less than D_{eq} in diameters. Assuming a constant crater production population, D_{eq} is always larger on older surfaces [e.g., *Gault*, 1970].

Evaluating the equilibrium state of crater populations, however, is still a challenge. The most frequently used method is by regarding certain empirical crater densities as the equilibrium level, i.e., once the density of a crater population has reached the empirical equilibrium level at a certain diameter, the crater population would be regarded as in equilibrium for diameters smaller than D_{eq}. An extreme case of crater equilibrium is geometric saturation, in which ideally same-sized craters on a given surface are in rim-to-rim configuration [*Gault*, 1970]. The cumulative SFD (expressed as $N = aD^b$, where a is the coefficient constant and b is the log-log slope) of a geometrically saturated crater population can be calculated based on the crater areal sizes as $N_{gs} = 1.54D^{-2}$ [*Gault*, 1970]. However, geometric saturation never actually occurs on any known planetary surfaces, because crater removal caused by continuous modification and destruction happens long before a possible rim-to-rim configuration could occur [*Melosh*, 1989]. The commonly referred empirical equilibrium density is that of *Gault* [1970], who performed several sand-box simulations of the crater accumulation process, and the production population in the simulations had a cumulative log-log slope (i.e., hereafter cumulative slope) of < -2. *Gault* [1970] found that crater population equilibrium occurred at 1–10% of the geometric saturation level, and the cumulative SFD slope of the crater population in equilibrium was about -2. Contemporarily, several observations of decimeter to hundreds of meters diameter craters on certain lunar surfaces [e.g., *Moore,* 1964], which were considered to be in equilibrium, suggested that their cumulative SFD all had a slope of about -2, and the densities were within the 1–10%N_{gs} level. Referring to those observations, *Gault* [1970] suggested that crater populations in equilibrium should always follow -2 cumulative SFD slopes. The 1–10%N_{gs} is possibly the correct equilibrium density range for most crater populations, because the crater density on the most heavily cratered surfaces of solar system bodies seldom reaches the 3–5%N_{gs} level [*Melosh*, 1989], although that range was derived from limited observations.

However, the empirical equilibrium density levels for different crater populations are poorly defined. Different equilibrium densities have been proposed for the same regions and/or the same production populations, e.g., *Gault* [1970] suggested ~2–4%N_{gs} for crater populations with production SFD slope < -2, and *Richardson* [2009] found ~5–10%N_{gs} for similar crater populations. However, some software packages (e.g., craterstats) prescribes the use of ~5%N_{gs} for all crater populations. *Hartmann* [1984] noticed that the crater SFD on the heavily cratered areas of the Moon, Mars, Mercury, and icy satellites were similar to each other within a factor of ~2–4, conforming to a power law fit of $N_H = 0.0468 \times D^{-1.83}$. This density level is also within the 1–10%N_{gs} range, and its approximate form that has a -2 cumulative slope is frequently used as the empirical equilibrium level for different crater populations. Referring to arbitrary equilibrium densities results in different interpretations for a given crater population. The lack of a clearly defined set of crater density values to indicate the existence of equilibrium conditions has produced frequently conflicting conclusions, particularly for crater populations on old surfaces and those with small diameters. For example, referring to the 10%N_{gs} equilibrium level would mean that the crater population on the average lunar highland is not in equilibrium for craters $\geq$20 km, but using the 5%N_{gs} equilibrium level indicates that the lunar highland has reached equilibrium for craters of at least 30 km diameter (see Figure S1 in the supporting information).

While any crater density (*not* SFD) at which equilibrium occurs can be expressed in the form of $N_{eq} = a \times D^{-2}$, the SFD of crater populations in equilibrium is affected by that of the production population [e.g., *Gault*, 1970; *Chapman and McKinnon*, 1986; *Richardson*, 2009]. When the production population has a cumulative slope of < -2, crater equilibrium is reached first by the smallest craters and after time the equilibrium diameter increases, with the crater population in equilibrium having a cumulative slope of about -2 [e.g., *Gault*, 1970; *Richardson*, 2009]. This equilibrium process is named the sand-blasting model [*Woronow*, 1977].

When the production population has a cumulative slope of > -2, larger craters have a greater potential of removing smaller craters, resetting regional cratering record and causing equilibrium at smaller diameters, a process called the cookie-cutting model [*Woronow*, 1977]. In this case, equilibrium is also indicated by smaller craters first and larger craters later, but the SFD of the crater population in equilibrium will roughly follow that of the production population with a cumulative slope of > -2 [e.g., *Chapman and McKinnon*, 1986; *Richardson*, 2009], although the density is lower than that of the production population. If in theory a production population would have a cumulative slope of -2, all the different-sized craters reach equilibrium at the same time [*Melosh*, 1989]. Within the crater count community, it has been a convention to assume that the crater populations in equilibrium will uniformly [*Gault*, 1970] or nearly [*Hartmann*, 1984] have a cumulative SFD slope of about -2. On the other hand, both analytical and numerical models have shown that some crater populations in equilibrium have cumulative SFD slopes larger than -2, such as those on the lunar highland [*Chapman and McKinnon*, 1986; *Richardson*, 2009]. However, the crater production in those models was the hypothesized primary crater populations (i.e., primaries), and the effect of contemporaneously produced secondary craters (secondaries), which may or may not dominate certain crater diameter ranges of the populations [e.g., *McEwen and Bierhaus,* 2006; *Werner et al.,* 2009] on equilibrium, was not included. On real planetary surfaces, crater equilibrium is caused by both primaries and secondaries. (In this study, the term production crater population does not distinguish between primaries and secondaries, unless the latter are obviously clustered, and those are excluded.) Therefore, the model results have to be tested by observational constraints.

Another method used to evaluate the equilibrium state of a crater population is by referring to the spatial distribution. Primaries form more or less randomly on planetary surfaces. For a population of primaries, equilibrium would cause more uniform spatial distribution due to continuous crater infilling and removal [*Lissauer et al.*, 1988]. Based on that hypothesis, several methods have been proposed to study the spatial randomness of crater populations and to evaluate their equilibrium states [e.g., *Squyres et al.,* 1997; *Kreslavsky,* 2007]. However, the reliability of these methods has not been systematically tested for crater populations in equilibrium.

Crater populations in equilibrium have lower densities at $D < D_{eq}$ than those of their production crater populations. Therefore, slope/density changes in crater SFD have also been used to deduce the equilibrium states of crater populations [e.g., *Shoemaker et al.,* 1969]. In reality, many other factors besides equilibrium can cause similar bendover of crater SFD. For example, resurfacing within the counting area [e.g., *Werner,* 2005], change of production SFD with time [*Strom et al.,* 2005], effects of layered target on cratering process [e.g., *Schultz et al.,* 1977], limited image resolution, and unfavorable illumination conditions when optical images were taken [e.g., *Young,* 1975] are all potential causes. Therefore, without detailed information of crater statistics (e.g., regional context and data used in the count), the equilibrium state of a crater population cannot be deduced solely from the slope change of crater SFD.

Here we analyze the crater populations of several young and old surfaces on the Moon. We first provide evidence that each crater population is in equilibrium for a part of the observed crater diameter range. We then compare the crater SFD for the crater populations. Integrating the geologic background and possible SFD for the production populations, we analyze factors affecting the crater equilibrium process, which have caused the observed SFD of the crater populations in equilibrium.

2. Methodology

We have selected several counting areas that have stratigraphic ages from the oldest to youngest on the Moon. Table S1 in the supporting information shows the detailed information of the counting areas. To ensure that the counting areas are homogeneous and no partial resurfacing events are detectable, surfaces with complex topographies and obvious secondary crater clusters and chains are avoided. For the counting areas that predate the Copernican epoch [*Wilhelms*, 1987], the Clementine Ultraviolet/Visible (UVVIS) color-ratio global mosaics [*Eliason et al.,* 1999] are also used to avoid heterogeneous areas, e.g., surfaces with different reflectance spectra and/or different optical maturity.

We have used the CraterTools toolbar [*Kneissl et al.,* 2011] for the crater counts. Each crater was manually collected by selecting three points on the crater rim. The central coordinates and diameters of the craters

were recorded. To study the crater SFD both within and larger than the diameter range in equilibrium and to ensure that the number of craters included in each area is statistically enough, the vertical and horizontal extents of each counting area must be at least 5 times larger than the diameter of the largest crater collected in the area. Images obtained by the Kaguya Terrain Camera (TC; ~7 m/pixel) [*Haruyama et al.,* 2008], Lunar Reconnaissance Orbiter Camera Wide Angel Camera (LROC WAC; 100 m/pixel), and narrow angle camera (LROC NAC; ~0.5–2 m/pixel) [*Robinson et al.,* 2010] have been used in this study. All the images have been calibrated following the standard processing procedure using the USGS Integrated Software for Imagers and Spectrometers (http://isis.astrogeology.usgs.gov/).

For a given crater population, the cumulative crater SFD would bend over toward a shallower slope when the crater diameter is close to the limit of image resolution. Although craters as small as several pixel sizes are exhaustedly searched in the counts, we have set a minimum confidence diameter of completeness (D_{min}) for each of the counting area, which is determined by the appearance of craters in the image used for the count. Basically, D_{min} is larger than 10 pixel sizes of the image. Moreover, it has long been noticed that images with smaller incidence angles and/or larger phase angles would obscure topographic contrasts, thus reducing the number of recognizable craters [e.g., *Young,* 1975]. To avoid the potential effect of image illumination conditions on crater statistics, we have used the same image data for counting areas that belong to the same geologic unit. Except for the Kaguya TC and LROC WAC global mosaics, the incidence angles of the images used are ~81°–88°, and the phase angles are ~70° (Table S1).

Different mathematical descriptions are available for presenting crater SFD (e.g., cumulative, incremental, and relative plots), and each has various weaknesses and strengths [*Crater Analysis Techniques Working Group*, 1979]. For crater populations that have included large numbers of craters, the relative plot (i.e., *R* plot) has the advantage in resolving subtle changes in the crater SFD. *R* plot shows the differential SFD with respect to a −3 slope, and the power law index (i.e., differential slope) is less than the cumulative slope by 1 [*Crater Analysis Techniques Working Group*, 1979]. To determine whether or not crater populations in equilibrium uniformly have about −2 cumulative SFD slopes, we have used the *R* plot to show the crater SFD for each of the counting areas. All differential slopes derived from *R* plots are exclusively translated to cumulative slopes for direct comparison.

3. Results

3.1. The Northern Rim of Tycho

Tycho ($D = 85$ km; 43°S, 11°W) is one of the youngest complex craters on the Moon as evident by its fresh ejecta rays. Possible ejecta deposits from Tycho were sampled by the Apollo 17 mission, and their radiometric ages indicate that Tycho might have formed at 109 ± 4 Ma [*Stöffler and Ryder*, 2001].

Tycho's continuous ejecta deposits are composed by the following three facies according to their morphology and overlapping relationship (Figure 1) [*Shoemaker et al.,* 1969]: (1) normal ejecta emplaced by both ballistic ejection and collapse of the transient crater, which have been mainly/solely modified by subsequent impact cratering since formation (Figure 1b); (2) melt veneers over restricted areas of normal ejecta, which have served as flow paths of impact melt (Figure 1c); and (3) small melt pools at local topographic lows, which were fed by surrounding melt veneers (Figure 1c). Using the same pair of LROC NAC images, we have selected a counting area for each of the three facies on the northern crater rim. The emplacement history of the three facies, which is reflected by their crosscutting relationships [*Osinski et al.,* 2011], is also shown by their crater SFD and densities, as (1) the normal ejecta deposits have the highest crater density, and the melt pools the lowest, and (2) the melt veneer has crater density similar to both the impact melt pools at $D = \sim 5$ m and the normal ejecta at $D = \sim 50$ m (Figure 1).

The SFD of the crater population on the normal ejecta can be divided into two: those with diameters larger than about 15 m have a cumulative slope of about −3 and those from 5–15 m diameter have a cumulative slope of about −2. A similar observation was noticed on another location of normal ejecta on the eastern crater rim [*Xiao and Strom*, 2012]. The change in the crater SFD slopes on the normal ejecta (i.e., $D > 15$ m versus $D < 15$ m) is not caused by the effect of target properties on different-sized craters, because the normal ejecta there have a thickness of at least dozens of meters estimated from empirical functions [*McGetchin et al.,* 1973], which is significantly larger than the excavation depths of the 5–70 m diameter craters,

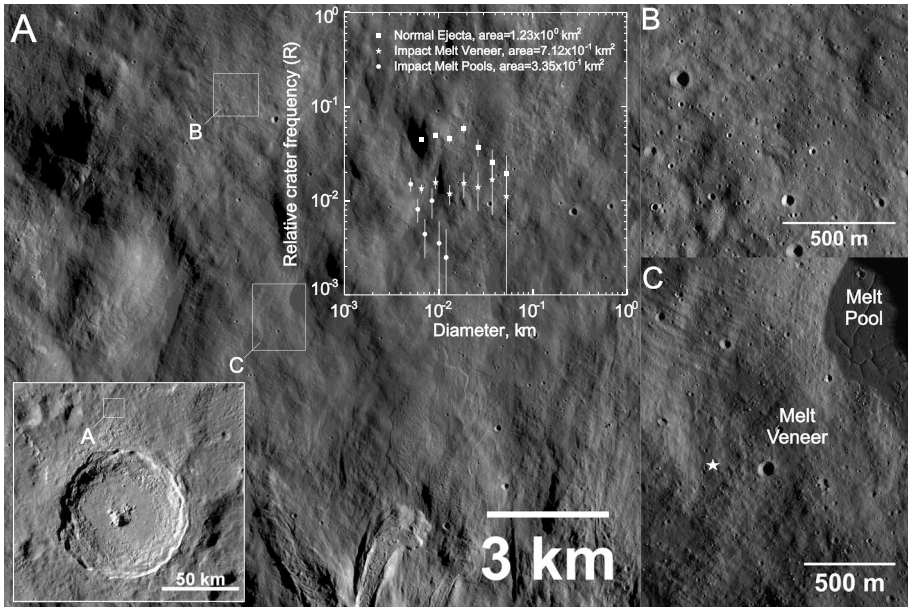

Figure 1. Tycho crater on the Moon and crater equilibrium on the continuous ejecta deposits. (a) Kaguya TC image of the north crater rim of Tycho shows the locations of the counting areas. The image in the lower left inset is from the LROC WAC global mosaic. (b) An example of normal ejecta that have mainly/only been modified by subsequent impacts since the emplacement. (c) The melt veneer and impact melt pool close to the landing site of Surveyor 7 (white star) [*Shoemaker et al.,* 1969]. Melt veneers are flow paths of impact melt over normal ejecta, and the melt eventually accumulated at local low relief areas forming melt pools. These two facies have less crater densities compared with the normal ejecta shown in Figure 1b. *R* plot of the crater size-frequency distributions on the three different ejecta facies is shown in Figure 1a. The images used in Figures 1b and 1c are from LROC NAC M131724362LE and M131724362RE (Mercator projection; 45.7 cm/pixel). North is toward up in all the images.

[*Holsapple*, 1993]. On the other hand, the melt veneer is a resurfaced unit over normal ejecta, and the observable crater population on the melt veneer has a cumulative slope of ~ −2 at D = 5–15 m. It can be inferred that prior to the emplacement of the melt veneer, the production crater population on the original normal ejecta would have a steeper SFD at D = 5–15 m (i.e., cumulative slope < −2). Moreover, the crater population that postdates the emplacement of the melt veneer has a cumulative slope of about −4, which is represented by the crater SFD on the melt pool (Figure 1). These lines of evidence together suggest that the flat segment (D = 5–15 m) of the crater SFD observed now on the normal ejecta cannot be the production population. After screening the possibilities, the D = 5–15 m crater population on the normal ejecta most likely represent the crater population in equilibrium, and the D > 15 m craters represent the production population. The crater populations on both the melt veneer and melt pools are not yet in equilibrium.

3.2. The Western Rim of Copernicus

The formation of the Copernicus crater (D = 96 km; 9.6°N, 20°W) represented the beginning of the Copernican epoch on the Moon [*Wilhelms*, 1987]. The Apollo 12 mission has sampled some material that was possibly ejected from Copernicus, and radiometric dating has yielded an age of ~800 ± 15 Myrs [*Stöffler and Ryder*, 2001]. The three different facies of the continuous ejecta deposits of Tycho are also identified on the rim of Copernicus, and those of Copernicus are more densely cratered (e.g., Figure 2b). To isolate the potential effect of different physical properties between impact melt pools and normal ejecta on crater statistics, we have selected four impact melt pools on the western rim of Copernicus, using the same NAC image pair (Figure 2). The four melt pools have comparable crater densities and SFD (Figure 2c). Within the diameter range of 5–100 m, the cumulative SFD slopes are about −2 generally. Small slope variations are visible in the crater SFD at different diameters, and the pattern of variations is the same on the four melt pools; craters with D < ~20 m have a cumulative slope of ~ −1.8, and craters with D = ~20–100 m have a cumulative slope of ~ −2.1 (Figure 2c).

At the diameter range of ~5–100 m, the production crater population on the melt pools of Copernicus probably had a cumulative slope of ≤ −3. The reasons are threefold: (1) The crater population formed on

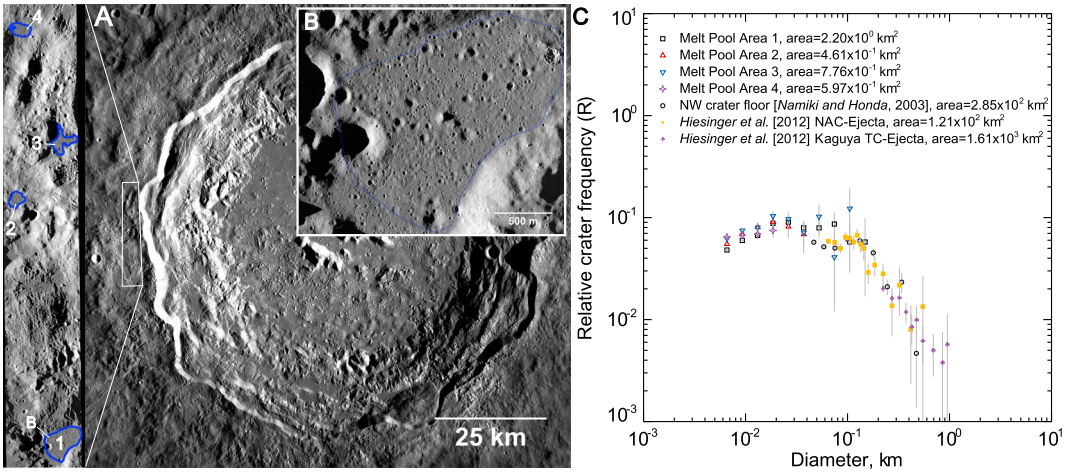

Figure 2. Copernicus crater on the Moon and crater equilibrium on the melt pools. (a) Kaguya TC mosaics show the Copernicus crater. The inset figure shows the locations of the four melt pools used in the count (areas 1–4 are numbered from the bottom to the top) on the western crater rim. (b) The Area 1 melt pool on the western crater rim. It is more degraded and heavily cratered than those on the rim of Tycho (Figure 1c). (c) *R* plot shows the crater size-frequency distributions on the four impact melt pools, together with those at larger diameters on the northwestern crater floor (data from *Namiki and Honda* [2003]) and normal ejecta (data from *Hiesinger et al.* [2012]). The base images for both the Figure 2b and the inset in Figure 2a are from LROC NAC M117637165LE and M117637165RE (Mercator projection; 59.8 cm/pixel). North is toward up in all the images.

the rim of Tycho probably has also formed on the rim of Copernicus, considering both the larger age of Copernicus and that their crater rims have comparable modes of ejecta emplacement as evident by the three same ejecta facies (Figures 1 and 2a). The production crater populations on the melt pools of Tycho have a cumulative slope of ≤ -3 at $D = \sim 5$–200 m (Figure 1) [see also *Xiao and Strom,* 2012, Figure 7]. At least this crater population has formed on the melt pools of Copernicus. (2) Craters larger than ~100 m diameter on both the normal ejecta [*Hiesinger et al.,* 2012] and melt pools (i.e., northern crater floor) [*Namiki and Honda,* 2003] of Copernicus have cumulative SFD slopes of ≤ -3 (Figure 2c). Therefore, the production crater population on the melt pools of Copernicus has possibly kept an overall steep SFD. (3) For the counting areas at Copernicus, the density of craters in the range of $D > 100$ m, where the crater SFD is steep, is comparable for the normal ejecta and melt pools, and that density is at least three times higher than that of same-sized craters on similar ejecta facies of Tycho (Figures 1 and 2c). In contrast, the normal ejecta facies of Tycho has a substantially higher crater density than Tycho's melt pools in the size range of $D = 5$–200 m (Figure 1) [see also *Xiao and Strom,* 2012, Figure 7]. This comparison suggests that the production crater populations on both the normal ejecta and melt pools of Copernicus probably had an overall steep SFD, and the larger age of Copernicus has allowed more craters to form on the melt pools, so that the initial density contrast between the normal ejecta and melt pools due to the emplacement of melt veneer (e.g., Figure 1) is no longer visible. The melt pools of Copernicus are unlikely to have been resurfaced after formation. Therefore, among all the possibilities, the observed overall flat SFD at $D = \sim 5$–100 m compared with the steeper SFD at larger diameters is most likely caused by equilibrium (i.e., $D_{eq} = \sim 100$ m). That is echoed by the heavily degraded appearance of craters within this diameter range (Figure 2b).

3.3. The Northern Sinus Medii

Sinus Medii (1.6°N, 1°E) is a small bay area ~600 km to the southeast of the Copernicus crater. At least four different episodes of mare basalts have filled this area as evident from their reflectance spectra [*Hiesinger et al.,* 2011]. The northern part of Sinus Medii has been treated as a standard calibration site of studying crater equilibrium on the Moon [e.g., *Marchi et al.,* 2012; *Minton et al.,* 2015]. The D_{eq} was interpreted to be ~200 m, based on the crater statistics of *Gault* [1970]. The original count was close to the landing site of the Surveyor 6 mission, but the precise location of the counting area was not provided. Estimates based on crater degradation models yielded an age of ~3.2–3.65 Ga for this area [*Boyce and Johnson*, 1978; *Fassett and Thomson*, 2014]. Numerous heavily degraded craters ≥200 m in diameter are visible in this area (Figure 3b). We selected two counting areas at the northern Sinus Medii using the same Kaguya TC image, which belong to the same

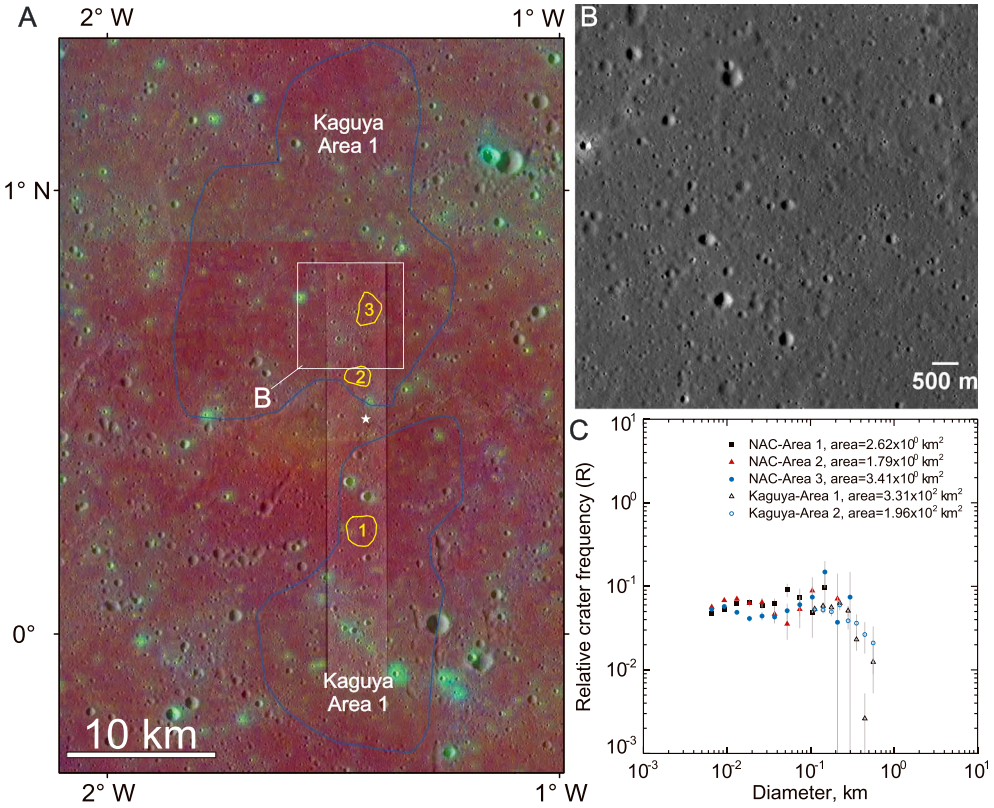

Figure 3. Crater equilibrium on the northern Sinus Medii. (a) Clementine UVVIS color-ratio mosaic over LROC NAC (M131657295LE and M131657295RE; 40.2 cm/pixel; Mercator projection) and Kaguya TC mosaics. The three yellow lines with annotated numbers are those selected from LROC NAC images (see Table S1 in the supporting information for detailed information of the counts). The northern Sinus Medii is largely homogenous seen in the color-ratio mosaic. The red, blue, and green channels of the color-ratio mosaic are reflectance ratios of 750 nm/415 nm, 750 nm/ 950 nm, and 414 nm/750 nm, respectively. The Surveyor 6 landing site is marked by the white star. (b) Numerous craters ~200 m diameters are heavily degraded on the northern Sinus Medii. The location of this area is shown in Figure 3a. The base image is from the Kaguya TC image TCO_MAPe04_N03E357N00E360SC (7.4 m/pixel; Mercator projection). (c) *R* plot shows the crater size-frequency distributions for the counting areas.

unit according to their reflectance spectra (Figure 3a). Three subregions were selected from the same pair of LROC NAC images (Figure 3a).

The two counting areas based on the Kaguya TC image have similar crater SFD and densities (Figure 3b). The same is true for the three small counting areas based on the LROC NAC images, although small variations are visible at several diameter bins, e.g., craters less than ~15 m diameter exhibit a cumulative SFD slope of −1.9 (Figure 3c). There is a major slope change in the crater SFD at about $D = 200$ m, as the slope is about −3 at $D \geq 200$ m, but smaller craters have a relative flat SFD with an overall slope of about −2. The result is similar to that of *Gault* [1970]. The steep crater SFD is consistent with that of the production population, considering that (1) the average crater population on the lunar mare has a cumulative slope about −3 at $D = 0.25$–4 km [*Basaltic Volcanism Study Project*, 1981], and (2) the $D \geq 200$ m crater population on Sinus Medii has a similar steep SFD slope to the $D \geq 100$ m crater population on the rim of Copernicus (Figure 2c), indicating that the production population probably maintained a SFD slope of about −3 on average.

The northern Sinus Medii predates Copernican units as evident from stratigraphic overlapping relationship [*Wilhelms*, 1987], which is consistent with the larger crater density at $D > 100$ m on the northern Sinus Medii (Figure 6). However, the two areas have comparable crater densities at the diameter range of ~5–100 m, and those at Copernicus have an even larger density at $D = \sim 10$–30 m (Figure 6). This comparison suggests that the overall flat crater SFD on the northern Sinus Medii does not represent the production crater population. Without detectable resurfacing events that could cause the slope change in the crater SFD, we concur with the interpretation of *Gault* [1970] that the $D \leq 200$ m crater population is in equilibrium (i.e., $D_{eq} = \sim 200$ m).

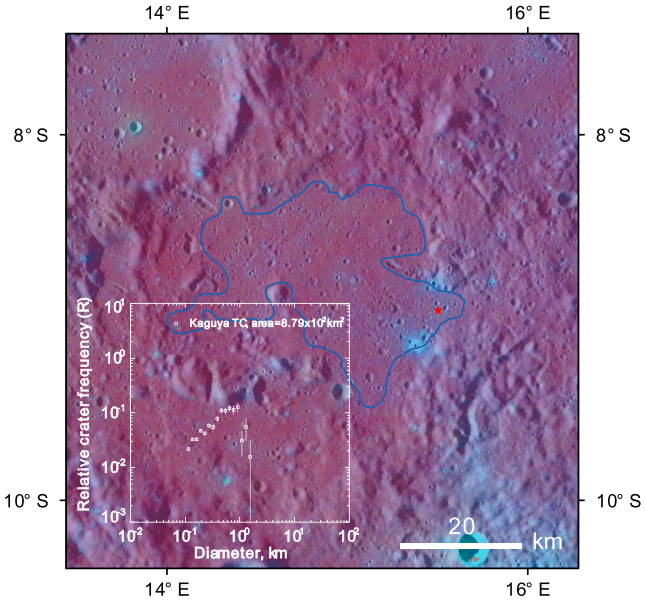

Figure 4. Crater equilibrium on the Cayley Plain. The Clementine UVVIS color-ratio mosaic over Kaguya TC mosaics confirms that the Cayley Plain is largely homogenous in reflectance spectra [*McKay et al.,* 1991]. The red, blue and, green channels of the color-ratio mosaic are reflectance ratios of 750 nm/415 nm, 750 nm/ 950 nm, and 414 nm/750 nm, respectively. The blue line is the boundary of the counting area, and the red star marks the Apollo 16 landing site. The *R* plot shows the crater size-frequency distribution on the Cayley Plain.

3.4. The Cayley Plain

The Apollo 16 mission landed on the Cayley Plain, which is fully covered by subdued overlapping craters with diameters larger than 700 m (Figure 4). Returned samples suggest that this plain was mainly composed by impact ejecta that were older than 3.86 Ga [*Stöffler and Ryder*, 2001]. The Cayley Plain postdates the Nectaris basin and predates the Orientale basin as evident from stratigraphic crosscutting relationships [*Spudis*, 1984], but the source basin(s) of the ejecta is still not confirmed [*Stöffler and Ryder*, 2001]. Little variations in albedo, other remotely sensed properties, and compositions of large rocks are visible within the Cayley Plain [*McKay et al.,* 1991], indicating that the plain has not been substantially resurfaced since the latest emplacement. We studied the crater population of 0.1–1.5 km diameter within the plain using the high-resolution Kaguya images. Areas of complicated topography are avoided (Figure 4), such as possible remnants of the Descartes Formation [*Spudis*, 1984]. Unlike previous studies that interpreted the Cayley Plain and two other nearby plains as one coherent geological unit [*Neukum*, 1983; *Robbins*, 2014], the plains that are close to the Cayley Plain and have similar spectral properties are not included in our count. This procedure decreases the size of the counting area, but it also reduces uncertainties caused by the possibility that these plains may not be same-aged units. Moreover, the reliability of the statistics is guaranteed by collecting all visible craters larger than 100 m diameter.

The crater SFD on the Cayley Plain can be divided into three segments, as the cumulative slope is about -1 at $D <$ ~500 m, -2 at $D =$ ~500–850 m, and < -3 at larger diameters (Figure 4). Several lines of evidence suggest that the $D <$ ~850 m crater population is most likely in equilibrium because the production population should have a SFD slope < -3 at this diameter range: (1) The production crater population on the lunar mare, which has a cumulative SFD slope of about -3 at $D = 0.2$–4 km [*Basaltic Volcanism Study Project*, 1981], has also accumulated on the Cayley Plain. The crater population with diameters larger than 850 m on the Cayley Plain also has a cumulative slope of < -3, indicating that the production crater population may have maintained an average SFD slope of < -3. (2) The Cayley Plain is older than the northern Sinus Medii, but craters less than ~200–300 m diameter on the Cayley Plain have a smaller crater density (Figure 6). Without apparent resurfacing events since emplacement [*McKay et al.,* 1991], the -1 cumulative slope at $D <$ ~500 m is unlikely to represent that of the production population on the Cayley Plain. (3) Most craters >700 m diameter on the Cayley Plain are heavily degraded, so that many similar-sized craters must have already been degraded beyond recognition.

3.5. The Most Heavily Cratered Terrain on the Lunar Highland

The lunar highland is composed of primary crustal material, but a large portion of it has been modified by subsequent basin forming and/or regional volcanic activity [*Jolliff et al.,* 2000]. To study the equilibrium state of the most ancient lunar highland, we selected an area at the western lunar farside that does not exhibit morphological or spectral evidence of subsequent volcanism or tectonism (Figure 5a). That area is away from large impact basins such as the South Pole-Aitken basin [*Jolliff et al.,* 2000], and it is situated outside the

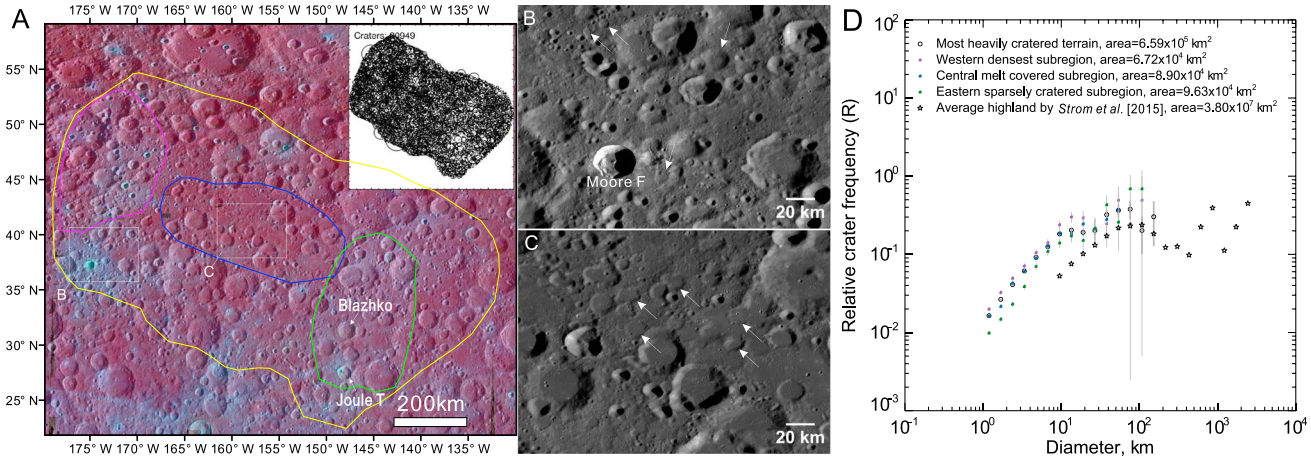

Figure 5. Crater equilibrium on the most heavily cratered terrain of the Moon. (a) Clementine UVVIS color-ratio mosaic over LROC WAC global mosaic shows the location of the counting area (yellow line). The inset figure shows the distribution map of the craters collected. The southeastern part of the counting area (green line) is relatively sparsely cratered compared with the other areas (e.g., violet line) due to the existence of some large fresh craters in this region, e.g., the Blazhko and Joule T craters. A small region in the center of the counting area (blue line) appears to have been partly covered by a veneer of smooth materials (Figure 5c), which may be impact deposits from nearby large craters (see text for explanation). (b and c) Parts of the counting areas. Numerous craters about 10 km and larger in diameter are heavily degraded (e.g., those pointed by the white arrows). The well-preserved Moore F crater ($D = 24$ km; Figure 5b) is annotated to show that the equilibrium state of a given area is depended on the research target, as the whole counting area in Figure 5 has been in equilibrium for crater populations at least 10 km diameter, the ejecta deposits of Moore F are not in equilibrium at this diameter range. The base images used in Figures 5b and 5c are from the LROC WAC global mosaic (100 m/pixel; equirectangular projection). The red, blue, and green channels of the color-ratio mosaic are reflectance ratios of 750 nm/415 nm, 750 nm/ 950 nm, and 414 nm/750 nm, respectively. (d) *R* plot shows the crater size-frequency distributions on both the whole counting area and the different sub-regions. Craters on the average lunar highland (data from *Strom et al.* 2015]) have a comparable shape of crater size-frequency distribution at diameters less than ~100 km.

continuous secondaries field [*Xiao et al.,* 2014] of the Orientale basin. The counting area has the highest crater density on the Moon for craters larger than both 20 km [*Head et al.,* 2010] and 64 km diameter (see Figure S2 in the supporting information).

For craters between about 1 and 100 km diameter in this area, we find a cumulative SFD slope of about −1. This is similar to that of craters ~10–100 km in diameter on the average highland [*Strom et al.,* 2015], but the counting area there has a much higher crater density (Figure 5). The distribution map of the craters there (inset in Figure 5a) shows that the western part of the counting area is one of the most densely cratered regions. The southeastern part has a relatively low crater density, which is probably caused by the a few relatively fresh craters larger than ~50 km in diameter (e.g., the Blazhko and Joule T craters) that have removed some small craters near these impact locations. In the center of the counting area, many craters about 10 km in diameter are subdued or half-buried by relatively smooth units (Figure 5c). Materials of these units have identical reflectance spectra with the surrounding terrain, and their occurrences are not correlated with topography (see Figure S3 in the supporting information). These materials may be ejecta deposits from nearby impact craters/basins, similarly observed on the Cayley Plain [*Spudis*, 1984]. The crater populations on the three subregions all exhibit SFD slopes of ≥ -1, but the western area has on average a larger crater density than the other two at $D \leq 10$ km (Figure 5d). Within a large homogenous area, crater degradation and obliteration caused by deposits from nearby craters (which belong to the same unit) could cause local crater density variations. Such crater removal is part of the processes causing equilibrium for the entire counting area. Therefore, the whole counting area shown in Figure 5a has a minimum D_{eq} of 10 km. That is consistent with the observation that numerous craters larger than 10 km diameters in this area are heavily degraded and their rims are barely identifiable (Figures 5b and 5c). It is also supported by modeling results showing that the crater population on the most heavily cratered regions of the Moon is likely in equilibrium for $D <=100$ km [*Minton et al.,* 2015].

4. Discussion

4.1. Processes Causing Crater Population Equilibrium

The equilibrium onset diameters and the cumulative SFD slopes of the crater populations in equilibrium on the five counting areas are summarized in Figure 6 and Table 1. Many of the results are consistent

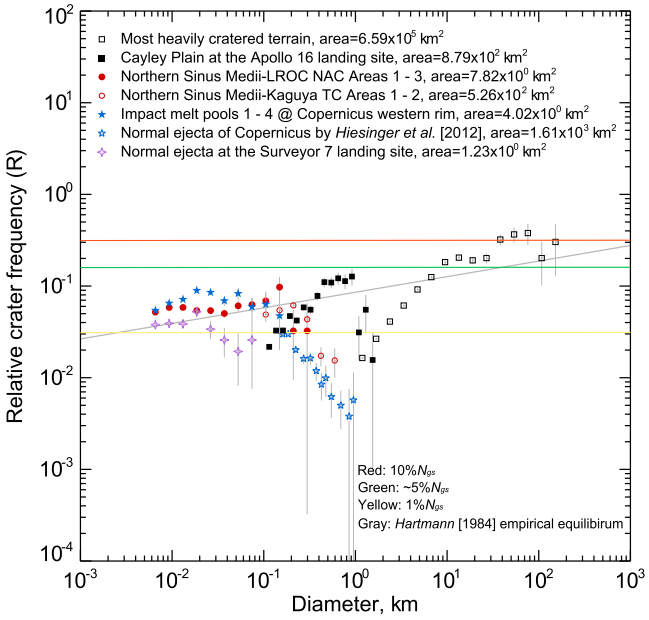

Figure 6. *R* plot compares the size-frequency distributions for the crater populations in this study. The four impact melt pools on the western crater rim of Copernicus, the three LROC NAC counting areas on the northern Sinus Medii, and the two Kaguya TC counting areas on the northern Sinus Medii are combined, respectively. Several prevalent empirical equilibrium density levels are compared with the crater counts. The results show that referring to empirical equilibrium densities is usually not reliable to evaluate the equilibrium state of crater counts.

with previous model predictions. For example, (1) the densities of the crater populations in equilibrium are mostly within the 1–10%N_{gs} [e.g., *Gault*, 1970]; (2) older surfaces generally have larger D_{eq} [e.g., *Gault*, 1970]; and (3) the SFD of crater populations in equilibrium is affected by that of the production crater population, as such crater populations have about −2 SFD slopes if those of the production populations are ≤−3 [e.g., *Soderblom*, 1970; *Woronow*, 1977], and the slope follows that of the production population if it is ≥−1 [*Chapman and McKinnon*, 1986; *Richardson*, 2009]. Such general consistencies suggest that the physical process causing crater population equilibrium is well constrained to the first order by previous models.

Cross comparisons of the crater populations studied here, however, show results that were not anticipated in previous models. For example, for the crater populations here whose production SFD slopes are ≤−3, although the crater populations in equilibrium have SFD slopes of about −2 in general, slope variations are identified at different diameter bins, e.g., the crater population in equilibrium at the Cayley Plain exhibits about −1 SFD slope at $D \leq$ ~500 m. Analytical models have argued that when the SFD slopes of production populations are ≤−3, the density at which equilibrium occurs is only related to the SFD slope of the production population [*Gault*, 1970; *Soderblom*, 1970], as steeper ones reach equilibrium at smaller densities. However, our results

Table 1. Summary of the Equilibrium States of the Crater Populations on the Counting Areas Shown in Figures 1–5

Counting Areas	Stratigraphic Age[a]	Equilibrium Onset Diameter	Cumulative SFD Slope of population in Equilibrium	Cumulative SFD Slope of Production Population[b]	Density Range of Craters in Equilibrium[c]	Small Variations Within the Diameter Range in Equilibrium
Most heavily cratered terrain	Pre-Nectarian	>10 km	~1	1 for D = 1–100 km	0.5–5.7%N_{gs}	Densities and SFD slightly vary at different locations
Cayley Plain	Nectarian	850 m	~2	≤3 for D = 0.07–1.5 km	0.6–3.9%N_{gs}	Densities and SFD vary at diameters larger and smaller than ~500 m
Northern Sinus Medii	Imbrian	200 m	~2	≤3 for D = 0.006–1 km	1.6–3.1%N_{gs}	Densities and SFD slightly vary at different locations and diameters
Copernicus ejecta and melt pools	Copernican	100 m	~2	≤3 for D = 0.006–1 km	1.7–2.8%N_{gs}	Densities and SFD slightly vary at different locations and diameters
Tycho ejecta	Copernican	15 m	~2	≤2.8 for D = 0.006–2 km	1.2%N_{gs}	-

[a]The stratigraphic ages are referred from *Stöffler and Ryder* [2001].
[b]For each of the counting areas, different crater populations that have different SFD [*Strom et al.*, 2015] may have formed. Here the cumulative SFD slope of the production crater population is for all the craters that have formed on the surface.
[c]The density ranges of the crater populations in equilibrium are presented in the form of percentages of the geometric saturation level (N_{gs}). For each counting area, the highest and lowest crater densities within the diameter ranges in equilibrium can be expressed as $N_{eq} = a \times D^{-2}$ (a is the constant). These density values are then transformed to derive the percentages of the geometric saturation level.

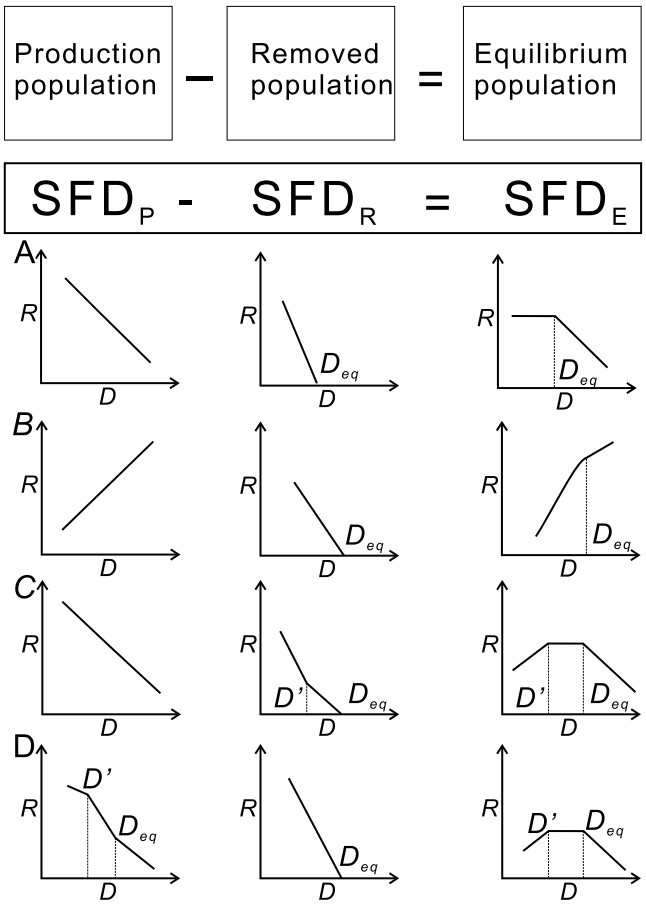

Figure 7. The size-frequency distribution of a crater population in equilibrium (SFD_E) is determined by that of the production crater population (SFD_P) and that of the removed crater population (SFD_R). This relationship is explained here using the four schematic models. All the SFD are presented in *R* plot. The diameter (*D*), *R* value, and SFD slope are only to relative sense, no absolute values is referred. D_{eq} denotes the equilibrium onset diameter for a crater population. *D*′ denotes the diameter less than D_{eq} from which the SFD of the crater population in equilibrium changes to different slopes. The production crater production is for all the craters (both primaries and secondaries) that have formed. (a) When the SFD_P has a cumulative slope of $\leq\sim -3$, crater equilibrium is mainly achieved by the sand-blasting effect caused by the vast amount of small craters [e.g., *Woronow*, 1977]. The crater population in equilibrium has an overall -2 slope at $D < D_{eq}$. (b) When the SFD_P has a cumulative slope of $\geq\sim -1$, crater equilibrium is mainly achieved by direct overlapping of larger craters, a process termed cookie-cutting effect [e.g., *Chapman and McKinnon*, 1986]. The SFD_E roughly maintains the slope of SFD_P at $D < D_{eq}$. In this case, the removed crater population has an unique SFD shape compared with that in the other panels, because when the production population has a cumulative SFD slope of $\geq\sim -1$, large craters have a high possibility of removing a significant portion of the surface, resetting the regional crater record, and dropping the overall crater density at small diameters. Different crater removal rates (Figure 7c) and production rate (Figure 7d) at different diameter ranges may cause small slope variations of SFD_E at $D < D_{eq}$.

show that the SFD slope of production population is not the only factor affecting the density of crater populations in equilibrium, e.g., the crater production on the normal ejecta of Tycho has a shallower cumulative slope than that at both Copernicus and Sinus Medii, but the equilibrium density is smaller at Tycho (Figure 6). Moreover, different-aged surfaces may have comparable densities (e.g., Copernicus versus Sinus Medii), and younger surfaces may have larger densities within diameter ranges of the crater population that are in equilibrium (e.g., Sinus Medii versus Cayley Plain). These observations suggest that besides the SFD of production crater population, other factors also affect the SFD of crater populations in equilibrium.

Crater equilibrium is achieved by continuous crater formation and removal. The SFD of crater populations in equilibrium (SFD_E) is controlled by that of the production population (SFD_P) and removed population (SFD_R). Vice versa, if the SFD_P is known, the SFD_R can be inferred from SFD_E. Previous models studied both crater production and removal and looked into the process leading to equilibrium from the perspective of SFD_P [e.g., *Hartmann and Gaskell*, 1997; *Richardson*, 2009]. In this work, we have adopted another perspective of view by emphasizing the combined effect of SFD_P and SFD_R. The schematic diagrams in Figures 7a and 7b show this relationship by assuming that the SFD_P has a single slope at all diameters. The first case shows (Figure 7a) that when the SFD_P has a slope of $\leq\sim -3$, a -2 slope of the observed SFD_E requires that the SFD_P has a steeper slope than that of SFD_P at $D < D_{eq}$. This equilibration process, which equals to the sand-blasting model [*Woronow*, 1977], is roughly consistent with that had happened on the normal ejecta of Tycho, considering that the SFD_P there had a slope of $\leq\sim -3$ at $D > 5$ m (Figure 1). The second case (Figure 7b) shows the cookie-cutting effect dominated by large craters when the SFD_P has a slope of $\geq\sim -1$, and this process can explain the equilibration process that had happened on the most heavily cratered terrain (Figure 5). The density of the crater population in equilibrium on the most heavily cratered terrain is an

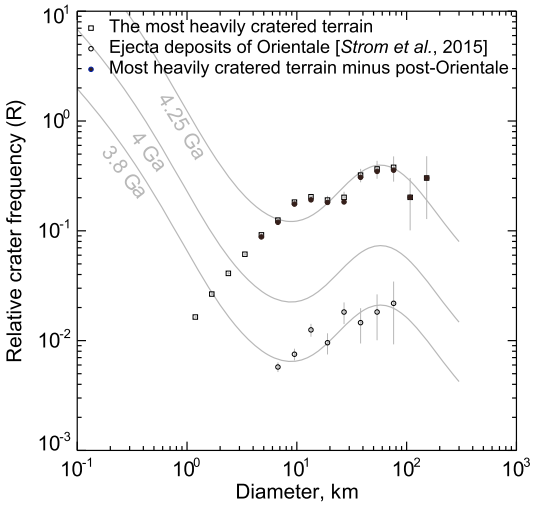

Figure 8. The crater population on the most heavily cratered terrain shown in Figure 5 has achieved the present equilibrium state before/during the Orientale basin was formed. The crater density on the most heavily cratered terrain is more than an order of magnitude larger than that on the ejecta deposits of the Orientale basin (data from *Strom et al.* [2015]). The subsequently formed crater population that postdated Orientale did not substantially affect the SFD or density of the crater population in equilibrium. The 3.8, 4, and 4.25 Ga crater isochrones (gray curves) are compared here to show that the production crater population before 3.8 Ga had a SFD slope of about −1 at $D = 10$–100 km. See also the SFD of the Population 1 craters in *Strom et al.* [2005]. The isochrones here are referred to *Neukum* [1983]. Note that many other versions of crater isochrones are available and they are different to some extents [cf. *Robbins,* 2014], but the shape of the crater production functions are more or less identical at $D = 10$–100 km [e.g., *Neukum et al.,* 2001].

order of magnitude larger than that of the crater population ($D = 5$–100 km) postdating the Orientale basin (Figure 8). Subtracting the post-Orientale crater population from the most heavily cratered terrain does not substantially change the density of the crater population in equilibrium (Figure 8). This comparison suggests that the most heavily cratered terrain had largely reached its present equilibrium state before/during the formation of the Orientale basin (~3.8 Ga), supporting that the impact flux before the formation of the Orientale basin was much higher than subsequent impacts [e.g., *Strom et al.,* 2005]. The production crater population on the lunar highland had a cumulative SFD slope of about −1 between $D = 1$ and 100 km [e.g., *Neukum et al.,* 2001], at least before about 3.8 Ga [*Strom et al.,* 2005]. Therefore, this crater population may have reached equilibrium according to the cookie-cutting model shown in Figure 7b.

Rather than the textbook models shown in Figures 7a and 7b [*Melosh*, 1989], both the SFD_P and SFD_R more probably have different slopes at different diameter ranges (e.g., Figures 7c and 7d) [*Richardson,* 2009]. That is because the SFD_P may have changed with time [e.g., *Strom et al.,* 2005; *Marchi et al.,* 2012], and different-sized craters may have different erosion rates [e.g., *Lucchitta and Sanchez,* 1975; *Schultz et al.,* 1977]. Their combined effects may cause the observed SFD_E exhibiting nonuniform slopes at $D < D_{eq}$. If the SFD_P has a roughly single slope at all diameters (Figure 7c), and some of the craters ($D < D' < D_{eq}$) have a faster removal rate than the rest of the craters ($D' < D < D_{eq}$), the SFD_E of the crater population in equilibrium at $D < D_{eq}$ will show two different slopes at $D < D'$ and $D' < D < D_{eq}$. An identical SFD_E as such can also be achieved if the SFD_R has a single slope (Figure 7d), and the SFD_P has a shallower slope at $D < D' < D_{eq}$ than that at $D' < D < D_{eq}$. The two schematic models, or their combined/intermediate cases, could explain the observed SFD_E at Copernicus, Sinus Medii, and the Cayley Plain, which all exhibit downturns at certain diameters ($D < D' < D_{eq}$; Figure 6). This downturn at $D < D'$ is not observed on the SFD_E of the normal ejecta of Tycho, at least for $D > 5$ m. It occurs at older terrains, and the downturn diameters are partly correlated with the relative regolith depths at these surfaces, i.e., the Copernicus < Cayley Plain and the Sinus Medii < Cayley Plain. Notably, a faster erosion rate for smaller craters is consistent with shorter lifetimes of smaller craters that are formed in thicker regolith [e.g., *Lucchitta and Sanchez,* 1975; *Schultz et al.,* 1977]. Also, local concentrations of large craters (e.g., the different subregions of the counting area shown in Figure 5) and seismic destruction caused by basin impacts [e.g., *Kreslavsky and Head,* 2012] could have similarly increased erosion rates for small craters. Therefore, at least a higher erosion rate at smaller diameters (Figure 7c) could potentially cause the observed two segments of SFD_E at $D < D_{eq}$ (Figure 6). This interpretation can also explain the following observations: (1) at some diameters, the crater population in equilibrium on the northern Sinus Medii has a lower density than that at Copernicus; (2) the crater population in equilibrium on the Cayley Plain has a lower density than that on the northern Sinus Medii at $D < 200$–300 m; and (3) After the most heavily cratered terrain had more or less reached the present equilibrium state before/at ~3.8 Ga (Figure 8), the subsequent steep production population on the Cayley Plain

($D < 1.5$ km) also formed on the lunar highland, but that younger population has not modified the SFD of the crater population already in equilibrium on the most heavily cratered terrain (Figure 6). That indicates a much higher erosion rate of the small craters (at least for $D < 1.5$ km) on the most heavily cratered terrain, which is consistent with the shorter lifetime of small craters formed within the much thicker regolith on the lunar highland [*Wilcox et al.,* 2005].

Our observations reveal that the SFD_E of the counting areas at Copernicus and the Northern Sinus Medii are an exception regarding the positive relationship between relative regolith thickness and D'. The D' of Copernicus (~18 m) is larger than that of the northern Sinus Medii (~11 m), but the average regolith thickness on the melt pools of Copernicus is less than that on the northern Sinus Medii considering the smaller age of Copernicus. This observation suggests that the SFD_P on the melt pools of Copernicus may have a shallower slopes at $D <$ ~18 m than that at 18 m $< D <$ 100 m. On the other hand, although the SFD_P of both the Cayley Plain and younger areas have average slopes of $\leq \sim -3$ within the studied diameter ranges (Figure 6), the slopes of SFD_R on these surfaces cannot be quantitatively compared due to the lack of knowledge on the relationship between regolith depth and crater removal rate. Therefore, the data presented here cannot adequately indicate the change of SFD_P with time.

In addition to the general, simplified models shown in Figure 7, several additional, specific models can be proposed, e.g., both the production and removed crater populations are likely have different SFD slopes at different diameter ranges. Nevertheless, the relationship of $SFD_P - SFD_R = SFD_E$ works for all planetary surfaces, considering the nature of processes causing equilibrium [e.g., *Gault*, 1970]. The production populations on the inner solar system bodies may have been largely similar [e.g., *Strom et al.,* 2005], considering different impact fluxes and variable target properties on different bodies. Due to the intensive bombardment prior to the formation of the Orientale basin (~3.8 Ga; Figure 8), crater populations on the inner solar system bodies may have reached equilibrium to diameters of at least $D_{eq} = 10$ km within the first 700 Myr (Figure 5). During this time, cookie cutting (Figure 7b) may be the dominate process causing crater populations to reach equilibrium on all the inner solar system bodies (although the detailed SFD_P is not well constrained) [*Werner,* 2014], so that their removed crater populations may have similar shapes of SFD_R at $D < D_{eq}$. Therefore, the crater populations in equilibrium on the most heavily cratered terrain on the inner solar system bodies may once had a cumulative slope of about -1, although subsequent degradation (e.g., erosion and volcanism) may have changed the SFD_E. This concept is consistent with both the model result of *Richardson* [2009] and interpretations for crater populations observed on both the lunar highland [e.g., *Hartmann,* 1984; *Head et al.,* 2010] and the heavily cratered terrain on Mercury [*Fassett et al.,* 2011]. On the other hand, for younger surfaces (i.e., the Cayley Plain and younger surfaces), the equilibrium states (e.g., D_{eq} and SFD_E) of the lunar crater populations studied here cannot be directly translated to same-aged terrains on the other solar system bodies. One of the important reasons is that although the younger SFD_P on different inner solar system bodies might have comparable shapes [*Strom et al.,* 2005, 2015], due to the much lower impact flux after ~3.8 Ga (Figure 8), crater removal caused by degradation processes that are not related with impact cratering (e.g., mass wasting) [*Xiao et al.,* 2013] becomes more significant in affecting the SFD_E. Surface modification processes on different bodies are not the same, e.g., fluvial and aeolian erosion processes occurred on Mars but not on the Moon or Mercury. That would cause different SFD_R and thus different SFD_E (Figure 7c). This effect is especially important when the SFD_P has an overall slope of $\leq \sim -3$, which is represented by crater populations less than 4 km diameter on the average lunar mare [*Basaltic Volcanism Study Project*, 1981]. In that case, crater equilibrium caused by sand blasting is effective, causing overall -2 slopes for SFD_E (e.g., Figure 7a) [*Richardson,* 2009], but slope variations in SFD_E (e.g., the D' in Figure 7) may not be identical on same-aged terrains on different bodies. For example, the larger impact flux on Mercury [e.g., *Minton and Malhotra*, 2010] may have caused larger D_{eq} than that on same-aged lunar surfaces due to accumulation of more craters in a given time. The 3 times larger average regolith thickness on Mercury [*Kreslavsky et al.,* 2014] may indicate a larger D' in the SFD_E than that of same-aged lunar surfaces. Processes causing crater degradation on Mars are more effective than those on the Moon or Mercury, so that the crater populations in equilibrium on Mars may more frequently exhibit SFD_E downturns at the $D < D' < D_{eq}$. Furthermore, the outer solar system bodies may have both different SFD_P [e.g., *Strom et al.,* 2015] and SFD_R with those of same-aged terrains on the Moon, so the SFD of crater populations in equilibrium on the outer solar system bodies can only be evaluated when integrating the observable SFD with the geological evolution of the counting areas.

4.2. Onset Diameter of Equilibrium and Surface Age

Crater populations in equilibrium have generally been disregarded when dating planetary surfaces. Our results suggest that D_{eq} is closely correlated with the age of the target surface, as older surfaces have larger D_{eq}, and same-aged surfaces that are younger than the Nectaris basin here have comparable D_{eq}. The potential of using D_{eq} as an indicator of relative or even absolute surface ages is promising when more D_{eq} are determined from a larger sample of variously aged surfaces.

The counting areas here are important calibration points in both lunar crater chronology models [*Stöffler and Ryder*, 2001] and the cratering history [*Wilhelms*, 1987]. Previous studies have built crater degradation models for lunar simple craters by only considering the effect of topographic diffusion [e.g., *Boyce and Johnson,* 1978; *Fassett and Thomson,* 2014], which is part of the processes causing crater equilibrium. The model ages were suggested to be consistent with those derived from crater densities, which were based on the lunar crater chronology model of *Neukum et al.* [2001]. The crater degradation models predicted that the maximum lifetime of a $D = 200$–300 m lunar crater was less than 3 Byrs, 800 Myrs for $D = 150$ m crater, and 70 Myrs for $D = 20$ m crater [*Fassett and Thomson*, 2014]. If the 109 ± 4 and 800 ± 15 Myrs sample ages were true for Tycho and Copernicus, respectively, the melt pools on the crater rims should have D_{eq} at least being 20 m and 150 m, respectively. Plus, crater degradation models estimated that the northern Sinus Medii was emplaced ~3.2–3.65 Ga, so that the D_{eq} should be much larger than 200–300 m [*Fassett and Thomson*, 2014]. However, the observed D_{eq} on these surfaces are much smaller (Table 1). Therefore, either the real ages of Tycho and Copernicus are substantially less than the prevalent sample ages and the crater chronology model of *Neukum et al.* [2001] may have indicated larger than real ages for a given crater population, or that the crater degradation models may have overestimated the surface erosion rate on the Moon due to the possibly nonlinear topographic degradation rates for craters larger and less than 800 m diameter [*Fassett and Thomson*, 2014]. The former, however, is disproved by recent work by *Werner and Medvedev* [2010] and *Werner et al.* [2014].

4.3. Spatial Distribution of Crater Populations in Equilibrium

Based on the crater populations in equilibrium studied here, we have tested the spatial analyses methods for detecting crater equilibrium [*Squyres et al.,* 1997; *Kreslavsky*, 2007]. The results show that most of the crater populations in equilibrium do not follow criteria for uniform spatial distributions (see Text S1 in the supporting information).

Both the theoretical reliability and practical plausibility of these methods need to be improved. Crater populations in equilibrium are usually simplified as points in the algorithms [*Squyres et al.,* 1997; *Kreslavsky*, 2007], but actual crater equilibrium is achieved by both two- and three-dimensional removal processes. More importantly, crater equilibrium on real planetary surfaces is achieved by both primaries and secondaries. Most crater populations in equilibrium may include some percent of unrecognized secondaries, which may cause spatial distributions deviating from randomness. Therefore, the spatial randomness of a crater population may not be strictly correlated with its equilibrium state. Performing both careful crater statistics and detailed geological study is, so far, the most reliable way to evaluate the equilibrium state of planetary surfaces.

5. Conclusions

We provide the first comprehensive observational constraint on crater equilibrium on the Moon since *Gault* [1970]. The SFD of crater populations in equilibrium on several young and old lunar surfaces are analyzed. Our results show that it is not reliable to evaluate the equilibrium state of crater populations by referring to arbitrary equilibrium densities, because the crater density at which equilibrium occurs is not correlated with the age of the crater population. Crater populations in equilibrium may have densities less than the 1% geometric saturation level of *Gault* [1970] at some diameters, which has been regarded as the minimum empirical equilibrium density level.

Besides the SFD of production crater populations, the crater removal rate of different-sized craters (i.e., SFD of removed crater population) also affects the SFD of the crater population in equilibrium. The cumulative SFD slope of crater populations in equilibrium is not always -2 when that of the production population is ≤ -3. Thicker regolith, local concentration of fresh large craters, and seismic destruction caused by large basins are some of the possible reasons for higher removal rates of small craters, affecting the SFD of the crater populations in equilibrium in a more variable manner.

The onset diameter where a crater population achieves equilibrium is positively correlated with the relative age of the crater population. For the counting areas younger than the Nectaris basin, the equilibrium onset diameter is the same at different locations of same-aged surfaces. The counting areas here are important calibration sites for both the lunar crater chronology models and the lunar cratering history. However, their equilibrium onset diameters are much smaller than those predicted by lunar crater degradation models, suggesting either that the crater erosion rate on the Moon is substantially less than the model estimation or that the prevalent crater chronology model of *Neukum et al.* [2001], calibrated with age-crater density pairs interpreted to relate to Tycho and Copernicus, overestimates surface ages.

Acknowledgments
The comments from the Associate Editor Gareth Collins and the two reviewers Simone Marchi and James E. Richardson Jr. helped to clarify the paper. This study is supported by the Research Council of Norway (235058/F20 CRATER CLOCK) and through the Centres of Excellence funding scheme, project number 223272 (CEED). The data used for this paper are available on request from the corresponding author.

References

Basaltic Volcanism Study Project (1981), *Basaltic Volcanism on the Terrestrial Planets*, 1286 pp., Pergamon, New York.
Boyce, J. M., and D. A. Johnson (1978), Ages of flow units in the far eastern maria and implications for basin-filling history, in *Proceedings of Lunar and Planetary Science Conference 9th*, pp. 3275–3283, Pergamon, New York.
Chapman, C. R., and W. B. McKinnon (1986), Cratering of planetary satellites, in *Satellites*, edited by J. A. Burns and M. S. Matthews, pp. 492–580, Univ. of Ariz. Press, Tucson, Ariz.
Crater Analysis Techniques Working Group (1979), Standard techniques for presentation and analysis of crater size-frequency data, *Icarus*, *37*, 467–474, doi:10.1016/0019-1035(79)90009-5.
Eliason, E. M., et al. (1999), Clementine: A global multi-spectral map of the Moon from the Clementine UVVIS imaging instrument, in *30th Lunar and Planetary Science Conference*, pp. 1933–1934, Lunar and Planetary Institute, Houston, Tex.
Fassett, C. I., and B. J. Thomson (2014), Crater degradation on the lunar maria: Topographic diffusion and the rate of erosion on the Moon, *J. Geophys. Res. Planets*, *119*, 2255–2271, doi:10.1002/2014JE004698.
Fassett, C. I., S. J. Kadish, J. W. Head, S. C. Solomon, and R. G. Strom (2011), The global population of large craters on Mercury and comparison with the Moon, *Geophys. Res. Lett.*, *38*, L10202, doi:10.1029/2011GL047294.
Gault, D. E. (1970), Saturation and equilibrium conditions for impact cratering on the lunar surface: Criteria and implications, *Radio Sci.*, *5*, 273–291, doi:10.1029/RS005i002p00273.
Hartmann, W. K. (1984), Does crater "saturation equilibrium" occur in the solar system?, *Icarus*, *60*, 56–74.
Hartmann, W. K., and R. W. Gaskell (1997), Planetary cratering 2: Studies of saturation equilibrium, *Meteorit. Planet. Sci.*, *32*, 109–121.
Haruyama, J., T. Matsunaga, M. Ohtake, T. Morota, C. Honda, Y. Yokota, M. Torii, Y. Ogawa, and the LISM working group (2008), Global lunar-surface mapping experiment using the Lunar Imager/Spectrometer on SELENE, *Earth Planets Space*, *60*, 243–256.
Head, J. W., C. I. Fassett, S. J. Kadish, D. E. Smith, M. T. Zuber, G. A. Neumann, and E. Mazarico (2010), The distribution of large lunar craters: Implications for resurfacing and impactor populations, *Science*, *329*, 1504–1507, doi:10.1126/science.1195050.
Hiesinger, H., J. W. Head, U. Wolf, R. Jaumann, and G. Neukum (2011), Ages and stratigraphy of lunar mare basalts: A synthesis, *Spec. Pap. Geol. Soc. Am.*, *477*, 1–51.
Hiesinger, H., C. H. van der Bogert, J. H. Pasckert, L. Funcke, L. Giacomini, L. R. Ostrach, and M. S. Robinson (2012), How old are young lunar craters?, *J. Geophys. Res.*, *117*, E00H10, doi:10.1029/2011JE003935.
Holsapple, K. A. (1993), The scaling of impact processes in planetary sciences, *Annu. Rev. Earth Planet. Sci.*, *21*, 333–373.
Jolliff, B. L., J. J. Gillis, L. A. Haskin, R. L. Korotev, and M. A. Wieczorek (2000), Major lunar crustal terranes: Surface expressions and crust-mantle origins, *J. Geophys. Res.*, *105*, 4197–4216, doi:10.1029/1999JE001103.
Kneissl, T., S. van Gasselt, and G. Neukum (2011), Map-projection-independent crater size–frequency determination in GIS environments—New software tool for ArcGIS, *Planet. Space Sci.*, *59*(11–12), 1243–1254, doi:10.1016/j.pss.2010.03.015.
Kreslavsky, M. A. (2007), Statistical characterization of spatial distribution of impact craters: Implications to present-day cratering rate on Mars, in *Seventh International Conference on Mars*, *Lunar Planet. Inst. Contrib. 1353*, pp. 3325–3328, Lunar and Planetary Institute, Pasadena, Calif.
Kreslavsky, M. A., and J. W. Head (2012), New observational evidence of global seismic effects of basin-forming impacts on the Moon from Lunar Reconnaissance Orbiter Lunar Orbiter Laser Altimeter data, *J. Geophys. Res.*, *117*, E00H24, doi:10.1029/2011JE003975.
Kreslavsky, M. A., J. W. Head, G. A. Neumann, M. T. Zuber, and D. E. Smith (2014), Kilometer-scale topographic roughness of Mercury: Correlation with geologic features and units, *Geophys. Res. Lett.*, *41*, 8245–8251, doi:10.1002/2014GL062162.
Lissauer, J. J., S. Squyres, and W. K. Hartmann (1988), Bombardment history of the Saturn system, *J. Geophys. Res.*, *93*(B11), 13,776–13,804.
Lucchitta, B. K., and A. G. Sanchez (1975), Crater studies in the Apollo 17 region, in *Proceedings of Lunar Science Conference, 6th*, pp. 2427–2441, Pergamon Press, Inc., New York.
Marchi, S., et al. (2012), The violent collisional history of asteroids 4 Vesta, *Science*, *336*, 690–693.
McEwen, A. S., and E. B. Bierhaus (2006), The importance of secondary cratering to age constraints on planetary surface, *Annu. Rev. Earth Planet. Sci.*, *34*, 535–567, doi:10.1146/annurev.earth.34.031405.125018.
McGetchin, T. R., M. Settle, and J. W. Head (1973), Radial thickness variation in impact crater ejecta: Implications for lunar basin deposits, *Earth Planet. Sci. Lett.*, *20*, 226–236.
McKay, D. S., G. Heiken, A. Basu, G. Blanford, S. Simon, R. Reedy, B. M. French, and J. Papike (1991), Lunar rocks, in *Lunar Sourcebook*, edited by H. Heiken, D. T. Vaniman, and B. M. French, pp. 183–284, Cambridge Univ. Press, Cambridge, U. K.
Melosh, H. J. (1989), *Impact Cratering: A Geologic Process*, pp. 1–255, Oxford Univ. Press, New York.
Minton, D. A., and R. Malhotra (2010), Dynamical erosion of the asteroid belt and implications for large impacts in the inner solar system, *Icarus*, *207*(2), 744–757.
Minton, D. A., J. E. Richardson, and C. I. Fassett (2015), Re-examining the main asteroid belt as the primary source of ancient lunar craters, *Icarus*, *247*, 172–190.
Moore, H. J. (1964), Density of small craters on the lunar surface, in *United States Geological Survey Astrogeology Studies Annual Program Report*, *Part D*, pp. 34–51, Gov. Print. Off., Washington, D. C.
Namiki, N., and C. Honda (2003), Testing hypotheses for the origin of steep slope of lunar size-frequency distribution for small craters, *Earth Planets Space*, *55*, 39–51.
Neukum, G. (1983), Meteoritenbombardement und Datierung planetarer Oberflachen, Habilitation thesis, Univ. of Munich, Germany.

Neukum, G., B. A. Ivanov, and W. K. Hartmann (2001), Cratering records in the inner solar system in relation to the lunar reference system, *Space Sci. Rev.*, *96*, 55–86, doi:10.1023/A:1011989004263.
Osinski, G. R., L. L. Tornabene, and R. A. Grieve (2011), Impact ejecta emplacement on terrestrial planets, *Earth Planet. Sci. Lett.*, *310*(3), 167–181, doi:10.1016/j.epsl.2011.08.012.
Richardson, J. E. (2009), Cratering saturation and equilibrium: A new model looks at an old problem, *Icarus*, *204*, 697–715.
Robbins, S. J. (2014), A new crater calibrations for the lunar crater-age chronology, *Earth Planet. Sci. Lett.*, *403*, 188–198, doi:10.1016/j.epsl.2014.06.038.
Robinson, M. S., et al. (2010), Lunar Reconnaissance Orbiter Camera (LROC) instrument overview, *Space Sci. Rev.*, *150*, 81–124, doi:10.1007/s11214-010-9634-2.
Schultz, P. H., R. Greeley, and D. Gault (1977), Interpreting statistics of small lunar craters, in *Proceedings of Lunar Science Conference, 8th*, pp. 3539–3564, Pergamon Press, Inc., New York.
Shoemaker, E. M., R. M. Batson, H. E. Holt, E. C. Morris, J. J. Rennilson, and E. A. Whitaker (1969), Observations of the lunar regolith and the Earth from the television camera on Surveyor 7, *J. Geophys. Res.*, *74*, 6081–6119, doi:10.1029/JB074i025p06081.
Soderblom, L. A. (1970), A model for small-impact erosion applied to the lunar surface, *J. Geophys. Res.*, *75*, 2655–2661, doi:10.1029/JB075i014p02655.
Spudis, P. D. (1984), Apollo 16 site geology and impact melts: Implications for the geologic history of the lunar highlands, *J. Geophys. Res.*, *89*, C95–C107, doi:10.1029/JB089iS01p00C95.
Squyres, S. W., C. Howell, M. C. Liu, and J. J. Lissauer (1997), Investigation of crater "saturation" using spatial statistics, *Icarus*, *125*, 67–82, doi:10.1006/icar.1996.5560.
Stöffler, D., and G. Ryder (2001), Stratigraphy and isotope ages of lunar geologic units: Chronological standard for the inner solar system, *Space Sci. Rev.*, *96*, 9–54, doi:10.1023/A:1011937020193.
Strom, R. G., R. Malhotra, T. Ito, F. Yoshida, and D. A. Kring (2005), The origin of planetary impactors in the inner solar system, *Science*, *309*, 1847–1850.
Strom, R. G., R. Malhotra, Z. Xiao, T. Ito, F. Yoshida, and L. R. Ostrach (2015), The inner solar system cratering record and the evolution of impactor populations, *Res. Astron. Astrophys.*, *15*(3), 407–434.
Werner, S. C. (2005), Major aspects of the chronostratigraphy and geological evolutionary history of Mars PhD thesis, Free Univ., Berlin, Germany. [Available at http://www.diss.fu-berlin.de/2006/33/indexe.html.]
Werner, S. C. (2014), Moon, Mars, Mercury: Basin formation ages and implications for the maximum surface age and the migration of gaseous planets, *Earth Planet. Sci. Lett.*, *400*, 54–65, doi:10.1016/j.epsl.2014.05.019.
Werner, S. C., and S. Medvedev (2010), The lunar rayed-crater population–characteristics of the spatial distribution and ray retention, *Earth Planet. Sci. Lett.*, *295*(1–2), 147–158, doi:10.1016/j.epsl.2010.03.036.
Werner, S. C., B. A. Ivanov, and G. Neukum (2009), Theoretical analysis of secondary cratering on Mars and an image-based study on the Cerberus plains, *Icarus*, *200*(2), 406–417, doi:10.1016/j.icarus.2008.10.011.
Werner, S. C., A. Ody, and F. Poulet (2014), The source crater of Martian Shergottite meteorites, *Science*, *343*(6177), 1343–1346, doi:10.1126/science.1247282.
Wilcox, B. B., M. S. Robinson, P. C. Thomas, and B. R. Hawke (2005), Constraints on the depth and variability of the lunar regolith, *Meteorit. Planet. Sci.*, *40*(5), 695–710, doi:10.1111/j.1945-5100.2005.tb00974.x.
Wilhelms, D. E. (1987), *The Geologic History of the Moon*, *U.S. Geol. Surv. Prof. Pap. 1348*, U. S. Gov. Print. Off., Washington, D. C.
Woronow, A. (1977), Crater saturation and equilibrium—A Monte Carlo simulation, *J. Geophys. Res.*, *82*, 2447–2456, doi:10.1029/JB082i017p02447.
Xiao, Z., and R. G. Strom (2012), Problems determining relative and absolute ages using the small crater population, *Icarus*, *220*, 254–267, doi:10.1016/j.icarus.2012.05.012.
Xiao, Z., Z. Zeng, N. Ding, and J. Molaro (2013), Mass wasting features on the Moon—How active is the lunar surface?, *Earth Planet. Sci. Lett.*, *376*, 1–11, doi:10.1016/j.epsl.2013.06.015.
Xiao, Z., R. G. Strom, C. R. Chapman, J. W. Head, C. Klimczak, L. R. Ostrach, J. Helbert, and P. D'Incecco (2014), Comparisons of fresh complex impact craters on Mercury and the Moon: Implications for controlling factors in impact excavation processes, *Icarus*, *228*, 260–275, doi:10.1016/j.icarus.2013.10.002.
Young, R. A. (1975), Mare crater size-frequency distributions: Implications for relative surface ages and regolith development, in *Proceedings of Lunar Science Conference, 6th*, pp. 3457–3473, Pergamon Press, Inc., New York.